SMU-HEP 04-08.
08/16/2004.

Liquid argon calorimeter calibration results from Front End Crate Test.

R. Stroynowski, J. Ye, P. Zarzhitsky*
Southern Methodist University, Department of Physics
Dallas, TX 75275-0175.

J. McDonald**
University of Pittsburgh, Department of Physics and Astronomy
Pittsburgh, PA 15260

F. Lanni
Brookhaven National Laboratory
Upton, NY 11973.

* contacting author; pavel@mail.physics.smu.edu
** jmcdon@hep.fsu.edu

.

1 Introduction.

ATLAS electromagnetic calorimeter will measure energy deposition produced by electrons and photons in the energy range from few GeV to few TeV [1]. The signals, in form of electrical charges due to ionization of the Argon atoms, are collected on the electrodes. The calibration system is needed to translate these signals into the corresponding loss of energy of the incoming particles.

Tests of the complete chain of the readout electronics were done at the Brookhaven National Laboratory from October 2003 to March 2004. This note describes the results concerning the calibration of the electronic readout.

2 Calorimeters - general consideration.

Calorimeters perform energy measurement of an incident particle by a total absorption and a conversion of the particle's energy into a measurable signal [2]. The calorimeter design can be optimized either towards the detection of electromagnetic or hadronic shower. The electromagnetic calorimeters are optimized for detection of electrons and photons while the hadronic calorimeters are optimized to measure showers produced by strongly interacting particles.

2.1 Electromagnetic calorimeters.

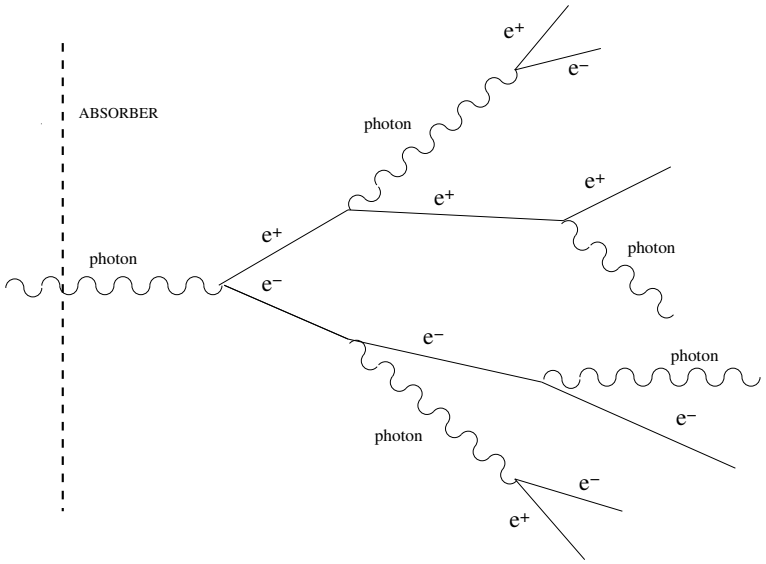

Figure 1: Electromagnetic shower development.

At energies above 1 GeV, an electron loses most of its energy through bremsstrahlung. The bremsstrahlung photon passing through the matter of the calorimeter undergoes conversion into

an electron-positron pair. Each electron and positron, in turn, can again emit the bremsstrahlung photons. These two processes repeat multiple times and produce a cascade of electrons and photons with decreasing energy. An illustration of the electromagnetic shower development is shown in Fig. 1. Two parameters describe electromagnetic shower in the way that is independent of the absorber material:

- The critical energy, E_c, is the energy at which the loss by radiation is equal to the loss by ionization (for electrons) and
- The radiation length X_0 is defined as the distance over which the energy of the electron is reduced by a factor of 1/e. The equivalent distance for photons is the mean free path X_γ, i.e., the distance after which the number of identical high energy photons has decreased by 1/e due to pair production. The relation between the mean free path and the radiation length is: $X_\gamma = 9/7 X_0$.

A 100 GeV shower deposits practically all of its energy in about 25 radiation lengths. Depth of the shower grows like $ln(E/E_c)$, so even at the LHC energies a calorimeter can be rather compact.

The lateral shower development is described by the, so called, Moliere radius

$$R_M = X_0 E_S / E_c,$$

where the constant $E_S = 21 MeV$. To a good approximation the Moliere radius is inversely proportional to the density. Typically, an infinite cylinder of a radius $2R_M$ contains 95% of the shower energy.

2.2 Hadronic calorimeters.

Hadronic showers are much more complicated than the electromagnetic ones. They result from the sequential inelastic hadronic interactions that produce cascades of different particles. A schematic illustration of a hadronic shower is shown in Fig. 2. Because the nuclear cross-sections are much smaller than that of the photon conversion, the hadronic showers start later in the material than the electromagnetic showers and, therefore, the hadron calorimeter must be more massive than the electromagnetic calorimeter. A part of the hadronic shower energy is released through electromagnetic component coming mostly from $\pi^0/\eta \to \gamma\gamma$ decays.

A longitudinal shower development is described by the interaction length λ, which is a mean free path between two inelastic nuclear interactions. The longitudinal shower size increases slowly with energy. For a 200 GeV hadron about 10 λ depth is required to deposit all of its energy. About 95% of the shower energy is contained in a radius of approximately 1 λ. The transverse profile of the shower consists of a narrow core of the e.m. component with a radius of about $2R_M$ and a broad hadronic tail.

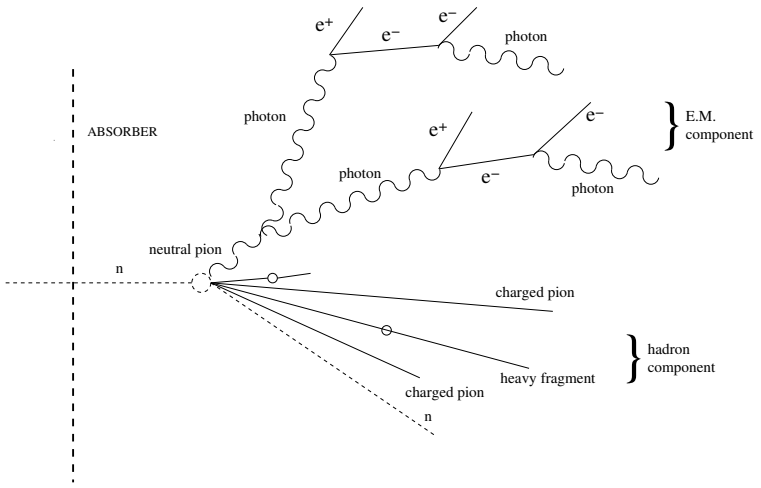

Figure 2: Hadronic shower development.

2.3 ATLAS electromagnetic calorimeter.

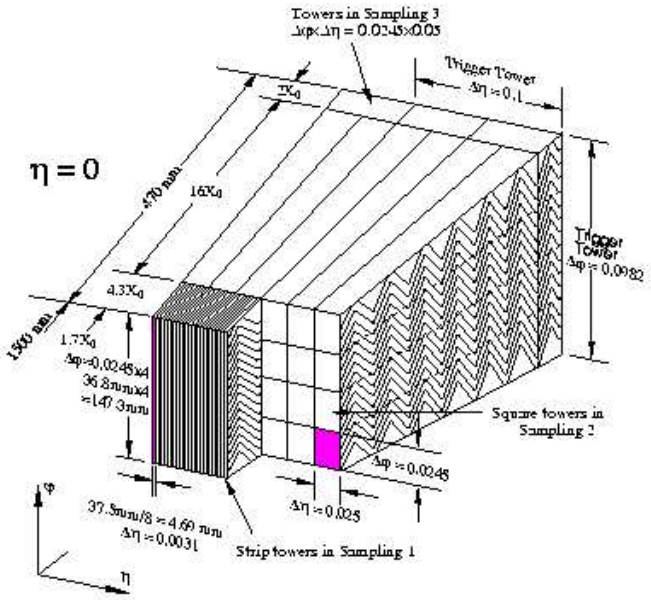

Figure 3: "Accordion-shaped" calorimeter cell.

The ATLAS electromagnetic calorimeter is designed to trigger on and to provide precision measurements of the energy of electrons, photons and missing E_T [3]. The last quantity describes an amount of a collision energy that escapes the detection in the calorimeter. Such missing

energy can be carried out by, e.g., neutrinos or a number of new particles expected in various extensions of the Standard Model: weakly interacting massive particles, stable supersymmetric particles and others. Beside the usual calorimeter tasks of energy and spatial measurements, the ATLAS electromagnetic calorimeter also provides angular measurements and participates in the particle identification.

The Liquid Argon sampling calorimeter with "accordion-shaped" electrodes is used for all electromagnetic calorimetry. It covers the pseudorapidity interval $|\eta| < 3.2$. A picture of the cell is shown in Fig. 3. The "accordion-shaped" electrodes produce a signal that is independent of the incident angle of the particle. In the sampling calorimeter the layers of the active medium alternate with the absorber layers. In the ATLAS calorimeter liquid Argon is used as an active medium and lead/stainless-steel plates are used as an absorber. The absorber plates have the thickness varying from 1.1 mm to 2.2 mm depending on the region. They are separated by the 2 mm gaps filled with the liquid Argon. The shower of a charged particle passing through the liquid Argon produces an ionization. The total charge collected on the cathodes is proportional to the energy deposited in the calorimeter.

The ATLAS calorimeter consists of a barrel part that covers azimuth of range $|\eta| < 1.475$ and two end-caps that cover a range $1.375 < |\eta| < 3.2$. The barrel and the end-caps cover a full 2π range in the polar angle. Total thickness of the e.m. calorimeter is above 24 X_0 for the barrel and above 26 X_0 for the end-caps and is divided into four layers in depth. This division allows us to study longitudinal profile of the shower that is needed in the particle identification.

3 Read-out electronics and calibration system.

3.1 ATLAS calorimeter read-out electronics system.

First of all, let's consider the chain of readout electronics of the LAr calorimeter and how the signal is changed when it is propagating through this chain [3]. The diagram of the electronics chain is shown in Fig. 4. A passage of a high energy particle generates a current signal in the calorimeter cell. This signal is called a physics signal. It is triangular in shape as a function of time. The integral of the signal over time or the total charge of this signal is proportional to the energy deposition.

A typical drift time of an electron through the 2 mm gap of the liquid Argon is 400 ns. At the LHC the bunch crossing will occur every 25 ns. The 400 ns drift time interval is long compared to the bunch crossing time and there may be overlapping signals from consecutive bunch crossings. To reduce the signal sensitivity to the noise and pileup effects at times significantly longer than the interval between the beam crossing, we take a derivative of the signal. The peak value of the differentiated signal is proportional to its total charge, i.e., to the energy deposited in the cell.

The calorimeter is placed in a cryostat that maintains a controlled low temperature necessary

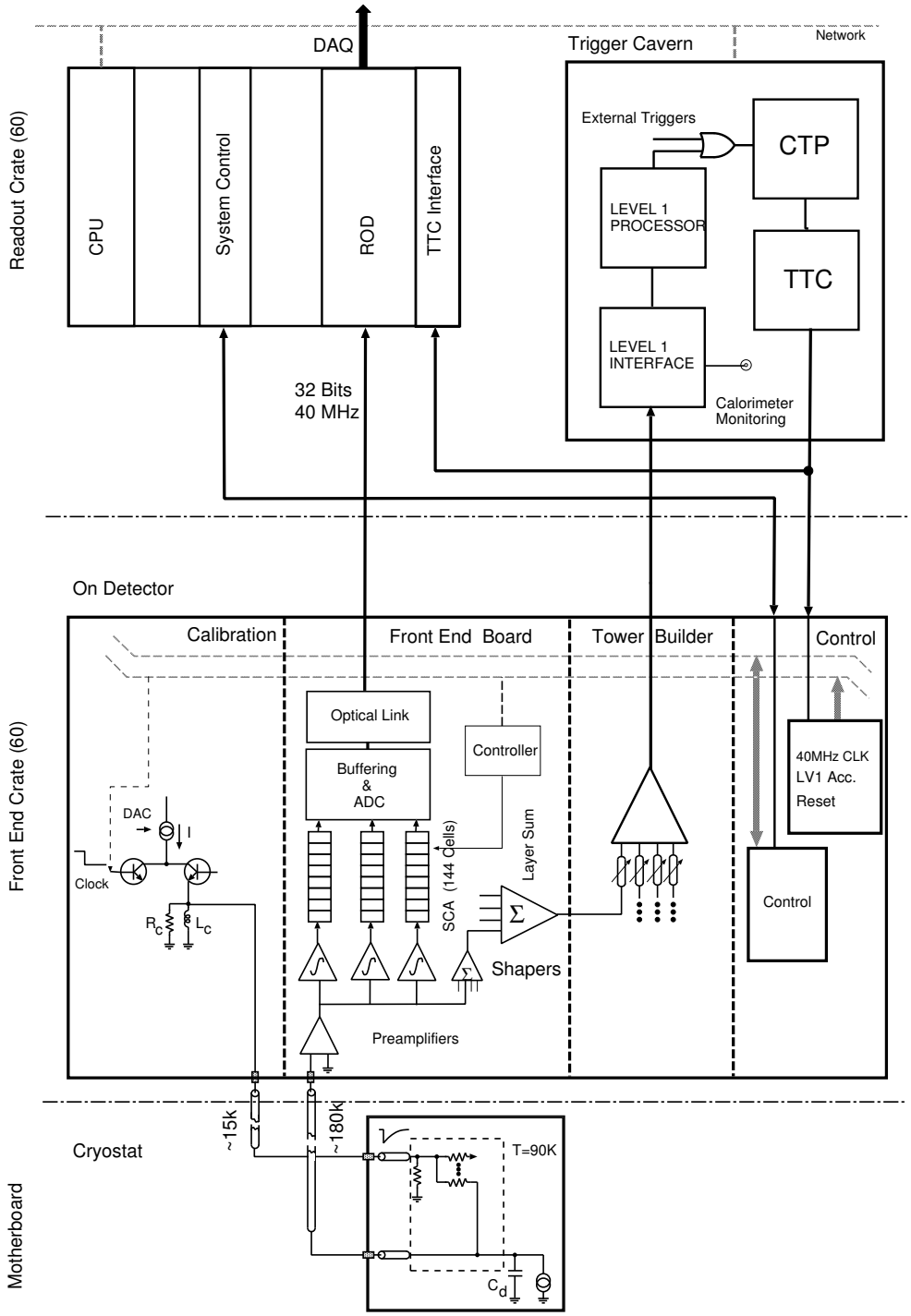

Figure 4: Diagram of the read out electronics chain.

for the liquid Argon. The signal collected on the electrodes is transmitted through a special cable system called a feedthrough outside the cold zone and then to the Front End Board (FEB). On the FEB, the current signal is first converted to voltage and amplified. Then the signal is differentiated by a shaping amplifier (shaper). In ATLAS, the shaper output signal is sampled every 25 ns and stored in a special analog pipeline, where it waits for the decision of the trigger. The calorimeter trigger uses a Tower Builder Board (TBB), that collects analog signals after the shaper, sums them to build trigger towers, and transfers trigger towers to the Level 1 Receiver system. The data wait in the pipeline, until the trigger makes a decision. If the event is triggered, a 12 bit ADC digitizes five samples of the signal in such a way that the third sample is within several nanoseconds from the peak. The shaping amplifier provides output with three different gains (1 - low, 10 - medium, 100 - high). The electronics automatically choose an appropriate gain value for the ADC input. These three gains allow us to use ADC more effectively by reducing the rounding error for small signals. The digitized signal samples are sent to the Read Out Driver (ROD) board. The signal after the ADC we will call a waveform.

3.2 ATLAS calorimeter calibration system.

The read-out electronics use a special calibration system. The main element of this system is a calibration board 4. This board can generate a calibration signal by a discharge of a large inductance. The calibration signal has an exponential shape and approximates well the triangular shape of the physics signal. The amplitude of the signal is defined by an input parameter called DACin. The DACin is a digital value on the 16 bit Digital to Analog Converter (DAC) that specifies a voltage on the inductance.

The calibration signal is injected as near as possible to the LAr gap where the physics signal is generated and then it is read and reconstructed through the corresponding cell readout chain. In this way the cell can be calibrated each time it is needed.

Though calibration and physics signals are very similar to each other they have a small but significant difference, that is caused by two reasons: one is the injected shape (exponential and triangular, respectively), the other is that they are injected in different locations. The calibration signal sees the circuit different than the physics signal, because its injection point is different. Therefore, these two signals are transformed differently by the beginning of the curcuit. That's why a correction method is needed to compensate the differnce between the calibration and physics signals.

3.3 FECT setup.

The Front End Crate Test (FECT) was carried out to test the complete electronics chain [4] of the ATLAS Liquid Argon calorimeter. A photo of the FECT setup is shown in Fig. 5. The setup, located at BNL, consisted of a complete unit of the electronics chain filling half of a front

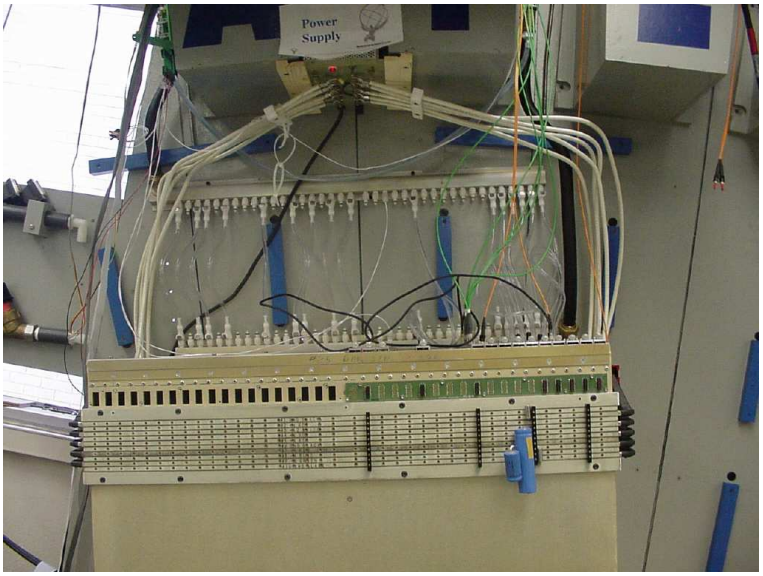

Figure 5: Photo of the FECT setup.

end crate. The effect of the real cells was simulated by appropriately chosen capacitors. The system contained 14 FEB's capable of reading 128 channels each, and the necessary control and service boards (crate controller, calibration board, tower builder board, clock distribution board, and monitor board). The boards were well shielded from the external noise by a Faraday cage. The FEB's were separated into four groups. Each group was processing signals corresponding to the one layer of the calorimeter. There was one board for the presampler (PS), seven boards for the front layer (F0 - F6), four boards for the middle layer (M0 - M3) and two boards for the back layer (B0 - B1). Because real cells were not available during the test, the calibration board was the only source of the input signal. Therefore, the results are valid only for the calibration signals and additional corrections are needed to compare them to those for the real data.

4 Optimal filtering.

The method of optimal filtering was chosen to calculate the energy corresponding to a measured calorimeter signal. This method is based on an assumption that the system is linear, and the shape of the signals differs only by an overall constant (amplitude), and that we know a normalized signal shape (master waveform) [5]. The calorimeter signal is an output signal of the shaper digitized by the ADC. A normalized waveform has the peak value equal to one. An example of a typical master waveform for the calibration signal is shown in Fig. 6.

In an ideal case knowing just the peak value of the signal should be enough to calculate the corresponding energy. But in practice we have to take into account the noise and the time

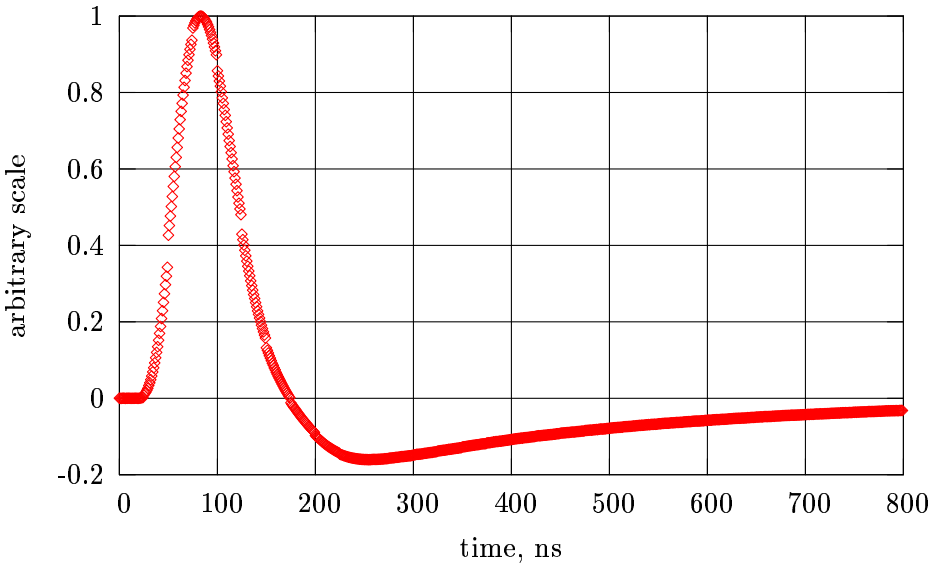

Figure 6: Master waveform.

jitter. Optimal filtering minimizes the effect of the noise and that of the jitter by using several points or samples of the signal. We use five samples to reconstruct energy from the Liquid Argon calorimeter signal.

If we assume that we know the signal shape and that the only uncertainties are its overall amplitude A and its time of origin τ, then the signal samples are given by

$$S_i = Ag(t_i - \tau) = Ag_i - A\tau g'_i + n_i,$$

where g is the corresponding master waveform, t_i is the sampling time and n_i is the noise component. Our goal is to find A and τ from the set of samples S_i, minimizing the effects of the noise. To do this, we define the coefficients a_i and b_i that are called optimal filtering coefficients (OFC). Using a_i and b_i, we can form two linear sums u and v:

$$u = \sum a_i S_i; \qquad\qquad v = \sum b_i S_i.$$

We choose coefficients in such a way that the expectation value of u is equal A and that of v is equal to $A\tau$. Thus we have

$$A =< u >= \sum(Aa_i g_i - A\tau a_i g'_i + < n_i >)$$
$$A\tau =< v >= \sum(Ab_i g_i - A\tau b_i g'_i + < n_i >)$$

The random noise will average to 0 leading to following constraints on a_i and b_i:

$$\sum a_i g_i = 1 \qquad\qquad \sum a_i g'_i = 0$$
$$\sum b_i g_i = 0 \qquad\qquad \sum b_i g'_i = -1.$$

The variances V of the parameters u and v are given by

$$V(u) = \sum a_i a_j < n_i n_j >= \sum a_i a_j R_{ij}$$
$$V(v) = \sum b_i b_j < n_i n_j >= \sum b_i b_j R_{ij}.$$

The expectation value $< n_i n_j >= R_{ij}$ is the noise autocorrelation function evaluated at a time $t_i - t_j$.

In order to get A and $A\tau$ we need to minimize the variances of u and v while satisfying the constraints for the optimal filtering coefficients. This can be done by using the method of Lagrange multipliers. The solution for OFC in a matrix form is

$$a = \lambda R^{-1} g + \kappa R^{-1} g'$$
$$b = \mu R^{-1} g + \rho R^{-1} g'$$

Here, λ, κ, μ and ρ are the Lagrange multipliers, $R = R_{ij}$ is the autocorrelation matrix and a, b, g, and g' are column vectors of optimal filtering coefficients, master waveform and its derivative respectively.

Solution for the Lagrange multipliers has a form

$$\lambda = Q_2/(Q_1 Q_2 - {Q_3}^2) \qquad \kappa = -Q_3/(Q_1 Q_2 - {Q_3}^2)$$
$$\mu = -Q_3/(Q_1 Q_2 - {Q_3}^2) \qquad \rho = Q_1/(Q_1 Q_2 - {Q_3}^2),$$

where $Q_1 = g^+ R^{-1} g$, $Q_2 = {g'}^+ R^{-1} g'$ and $Q_3 = {g'}^+ R^{-1} g$.

When we know OFC, the amplitude A and the start time τ can be easily calculated from the signal samples using equations:

$$A = \sum a_i S_i$$
$$A\tau = \sum b_i S_i.$$

5 Experimental data taking.

In order to reconstruct the energy deposited in the calorimeter from a calorimeter signal, we need to know the Optimal Filtering Coefficients (OFC). To obtain the OFC, we need to know the master waveform, its derivative and the noise autocorrelation function. All this information can be obtained from the calibration procedure.

The calibration system allows for the precise measurements of the calibration waveform for each channel. The calibration waveform is a waveform that is generated when the input signal originates from the calibration board and not from the physics process. The read-out system allows us to measure the signal every 25 ns. The calibration board provides an identical input signal as many times as we want. By delaying the input signal we can sample a different set of points of the same waveform. This procedure is called a delay run. By measuring 25 delay

runs with identical input signals, that are consecutively shifted by 1 ns each with respect to the previous one by the calibration board, we obtain a set of samples of the calibration waveform for every nanosecond interval. During FECT we took 200 identical events for each point of the each calibration waveform. The value of the waveform was obtained by averaging over these identical events to minimize random fluctuations.

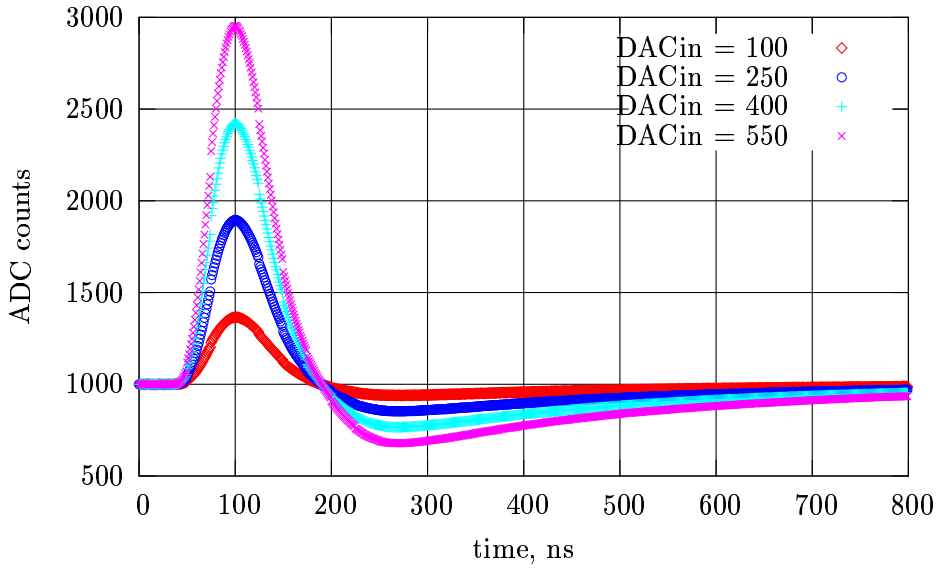

Figure 7: The calibration waveforms corresponding to different DACin.

To calculate a master waveform we need to measure several calibration waveforms with different values of the amplitude or DACin. Four calibration waveforms corresponding to different DACin are shown in Fig. 7. Next, for each point of the master waveform we fit to a linear function the calibration waveform values at this point versus the DACin values corresponding to these calibration waveforms. An example of the fit is shown in Fig. 8. The slope of the fit represents a value of the unnormalized master waveform. The waveform is normalized in such a way that its peak value is equal to one. After the normalization we get the master waveform that is used for the OFC calculation. A typical master waveform and its derivative are shown in Figs. 6 and 9.

In order to calculate the noise autocorrelation matrix, we took data during a special run with the readout system turned on but without any input signal. In this case the only source of the signal was the noise in the electronic chain. We took 100,000 events, and obtained the autocorrelation matrix by averaging over these events. The quantity R_{ij} equal to the product of responce in the same channel at times t_i and t_j. $R_{ij} =< n_i n_j >$. We took separate runs to obtain R_{ij} for all three gain values.

Each of the 14 different FEB boards has 128 independent channels. Every FEB channel

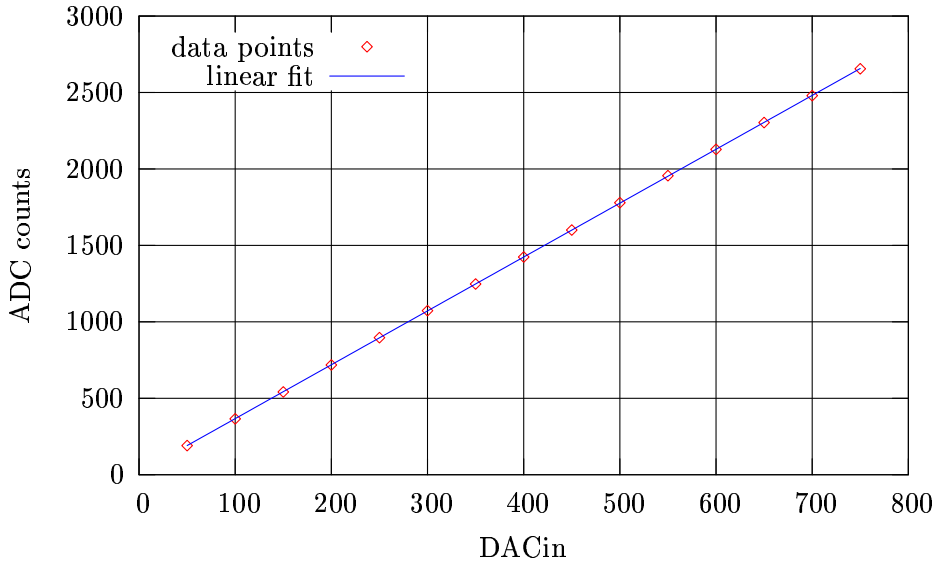

Figure 8: An example of the master waveform fit.

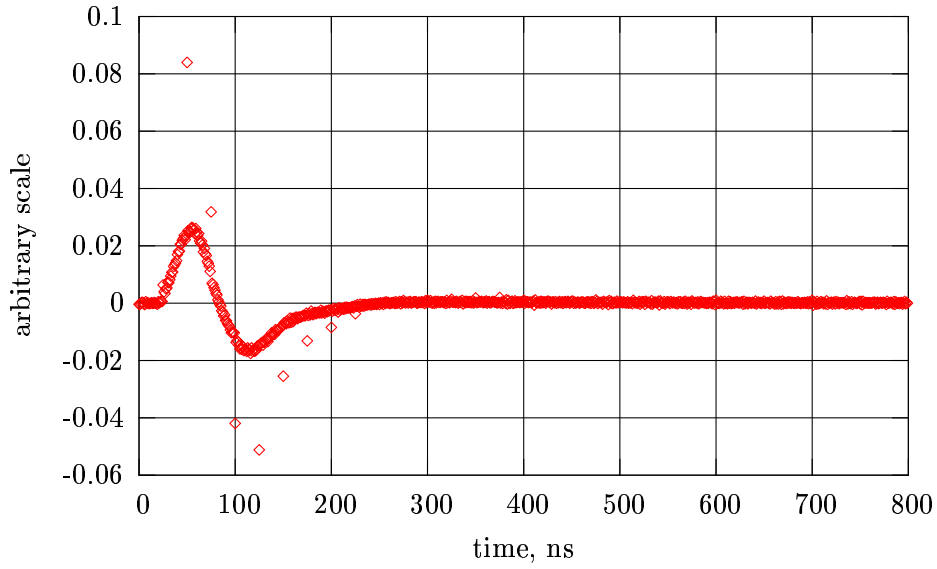

Figure 9: Derivative of the master waveform.

needs to be calibrated differently. A complete calibration run includes several sets (about 15) of 25 delay runs with different DACin values for each FEB. During the FECT, three complete calibration runs for high and medium gains, and two complete calibration runs for low gain were taken with the final setup.

6 Data analysis.

6.1 Linearity of the system.

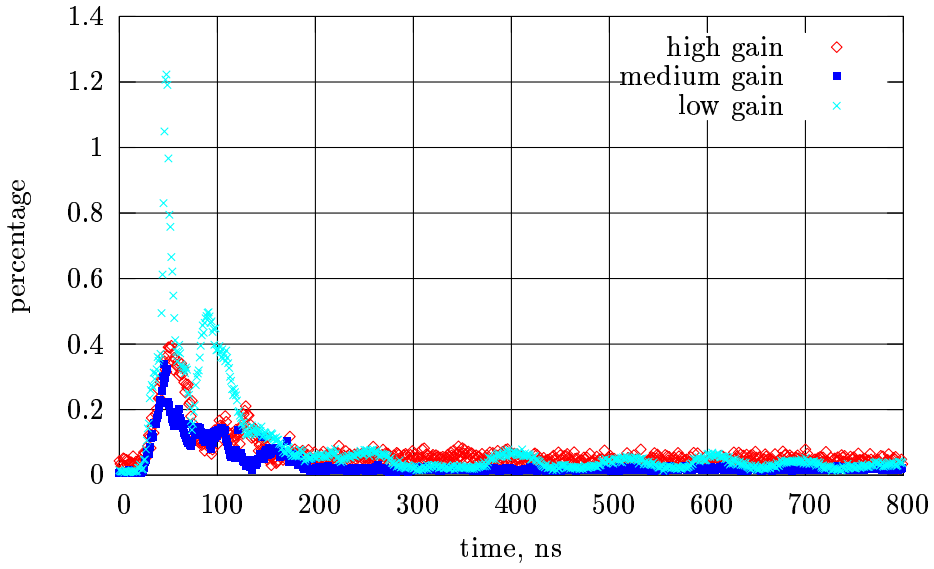

Figure 10: Integral nonlinearity of the master waveform fit.

The optimal filtering method uses an assumption that the system is linear. The ATLAS requirement is that the integral nonlinearity of the master waveform fit must be smaller than 1%. The integral nonlinearity is the absolute value of the maximum difference between the fit and the data divided by the maximum of the largest calibration waveform in the channel. In the Fig. 10 you can see a typical nonlinearity for the high gain. High and medium gain data satisfy the requirement. Low gain data have some problems with linearity, that will be discussed later.

6.2 Delay step results.

The master waveform shown in Fig. 6 has discontinuities every 25 ns. We have verified that these gaps are caused by the fact that, during the delay run, the actual delay steps are not exactly equal to 1 ns. The corresponding time error is cumulative and proportional to the delay value. As a consequence, we put the master waveform points in the wrong time positions. Thus the point that corresponds to a delay value of 24 ns is substantially shifted in time while its neighboring point corresponding to a delay 0 is not shifted at all. Hence, the difference in time between these two adjacent points can be much bigger than the nominal value of 1 ns creating the observed discontinuities of the master waveform.

During the FECT we made measurements of the exact delay values coming from the calibration board using a scope. We then corrected the corresponding time intervals for our mea-

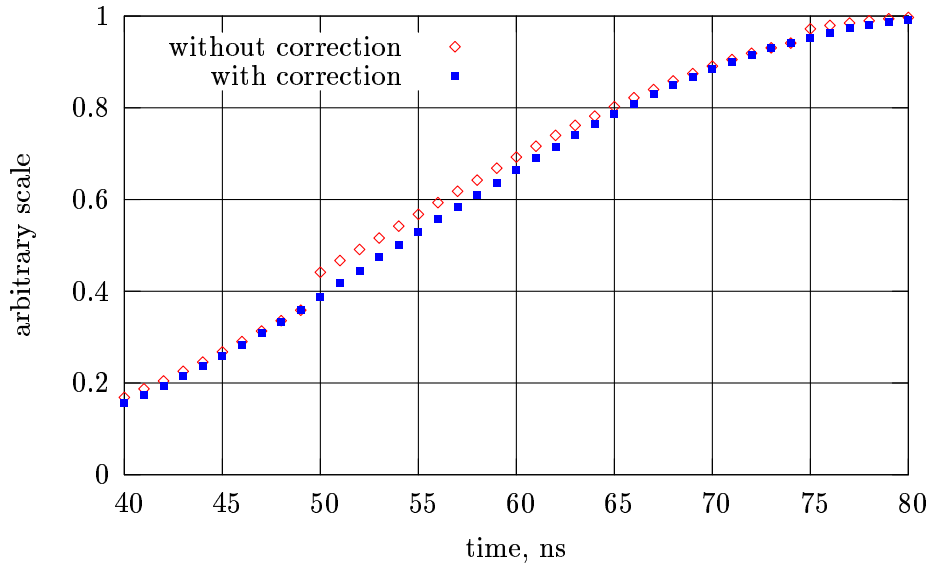

Figure 11: Part of the master waveform without correction and with different corrections

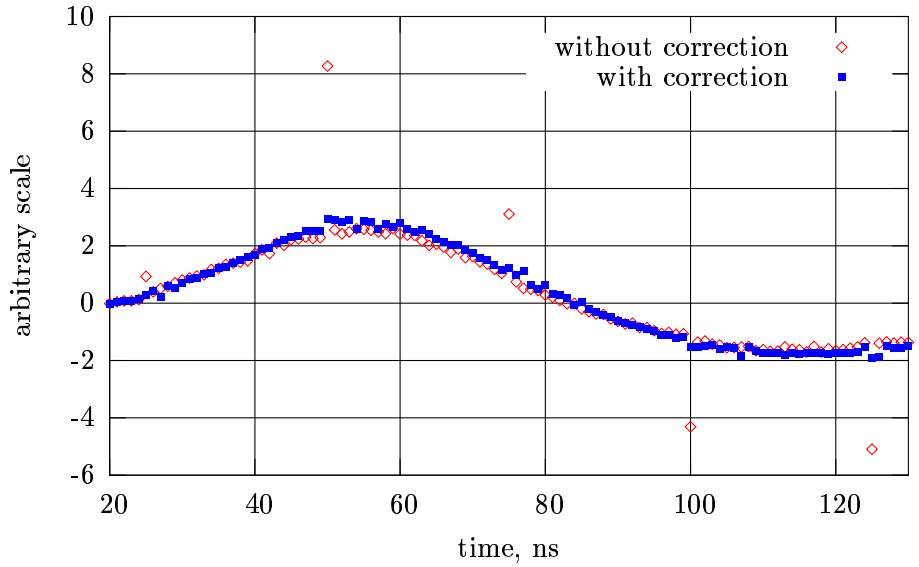

Figure 12: Derivative of the master waveform with and without corrections

surement. The corrected master waveforms and their derivatives are shown in Figs. 11 and 12 together with original, uncorrected measurement. The corrections compensate well for the discontinuities in the waveform and its derivative. To avoid this problem in the subsequent measurements, it was decided to use delay values from the TTCRx board.

6.3 Report on problems found.

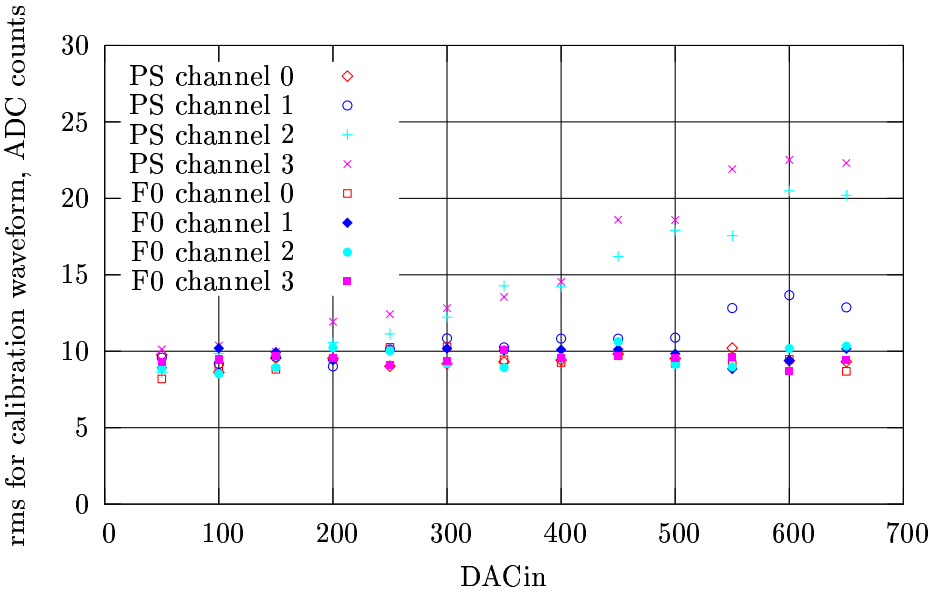

Figure 13: Comparison of calibration waveform rms for PS and F0.

An unexpected dependence of the root-mean-square (rms) for the calibration waveforms on the input DACin values was found for the PS board. The comparison of the rms for the PS and the F0 boards is shown in Fig. 13. The rms is growing with increasing DACin value for several channels of the PS board while it is approximately constant for the F0 board.

The input calibration signals are generated by 128 pulsers located on the calibration board. The PS board is calibrated using only four out of the 128 pulsers located on the calibration board the results illustrated in Fig. 13 can be grouped into four clases each corresponding to the same pulser. The rms growth with the increasing DACin value differs for each group. It is smallest for the group corresponding to pulser #1 and largest for the group calibrated by pulser #4.

As can be seen in Fig. 14, the largest growth corresponds to the maximum of the the signal. We conclude that the effect is proportional to the amplitude of the signal.

The previous data were taken with all 14 FEB's working simultaneously and all 128 pulsers on the calibration board active. When only the PS board and its four pulsers are active, there is no growth of rms with DACin. This is shown in Fig. 15. The corresponding dependence for PS and F0 are the same. We conclude that the effect is proportional to the signal and all FEB channels corresponding to the same pulser have the same behavior. The effect disappears when we enable only four out of 128 pulsers. This demonstrates that the effect is caused by a cross-talk between the calibration channels.

A similar problem exists for all boards at low gain. Because of the large current needed for

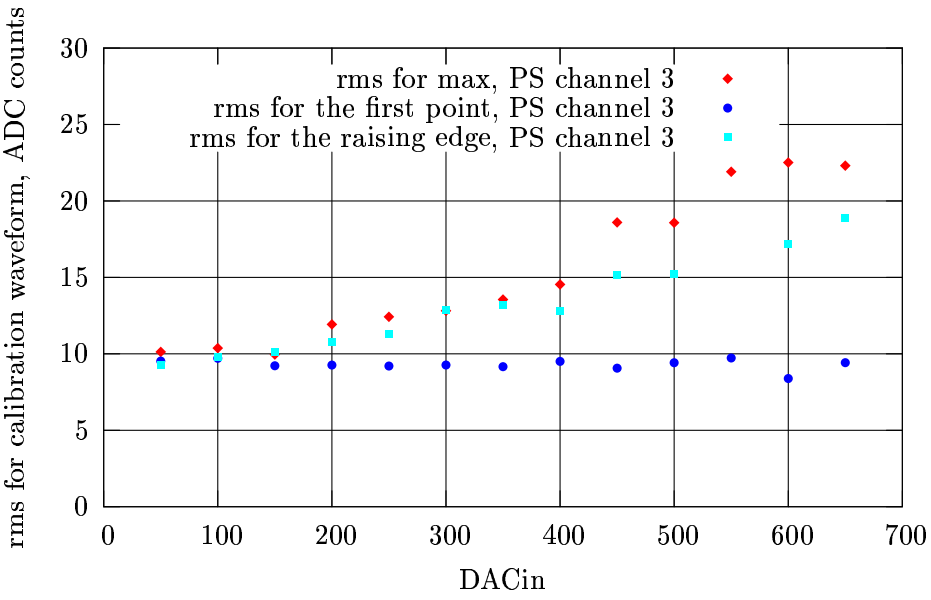

Figure 14: Comparison between rms for different points on calibration waveform rms for PS.

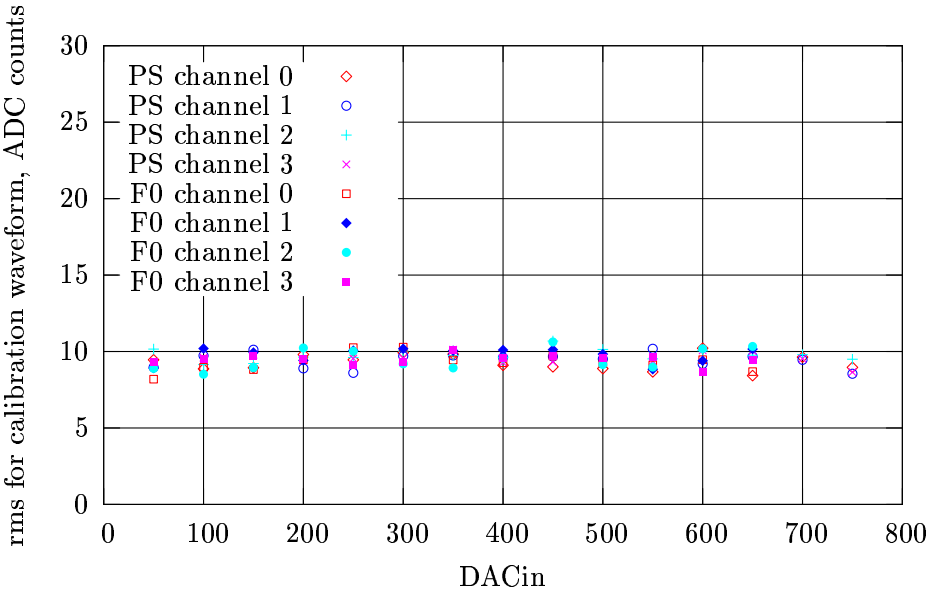

An unexpected dependence of the root-mean-square (rms) for the calibration waveforms on the input DACin value was found for the PS board.

Figure 15: Comparison of calibration waveform rms for PS with only PS active and F0.

the calibration at the low gain, not all FEB's data were taken at the same time. The data for F1, F2, F3 and for F4, F5, F6 were taken simultaneously. The data for all other FEB's were taken for one board at a time. However, even in this case the integral nonlinearity for all boards

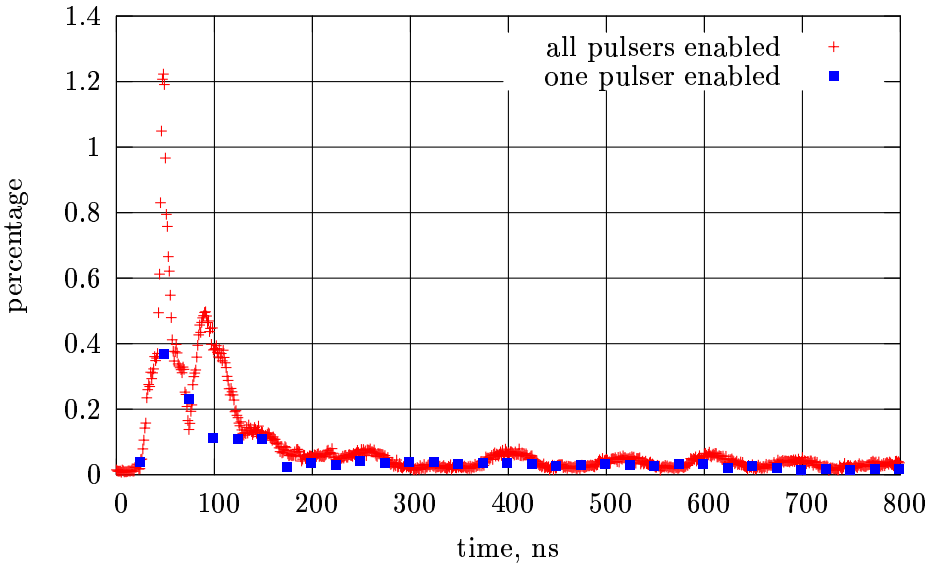

Figure 16: Example of the integral nonlinearity for one of the channels for PS board.

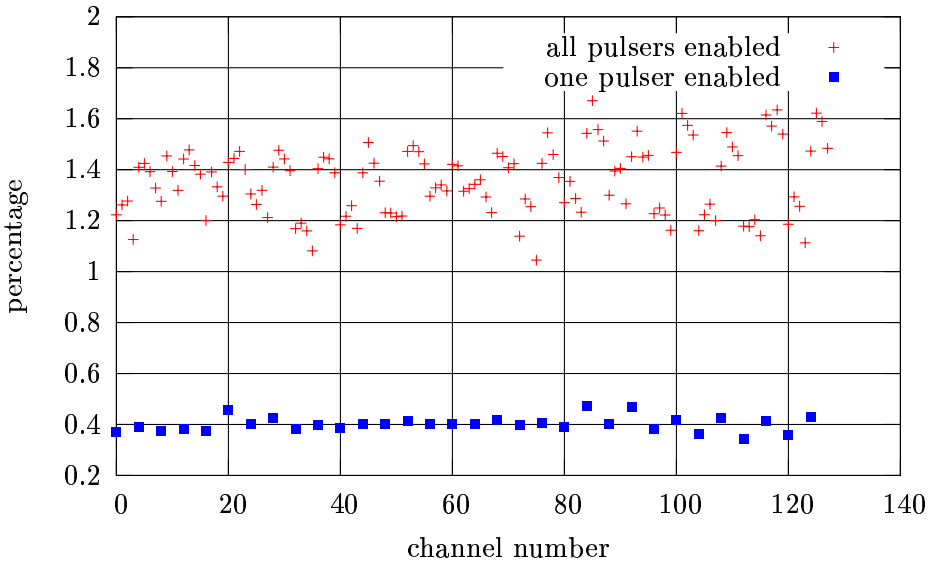

Figure 17: Maximum integral nonlinearity versus channel number for PS board.

is larger than 1%.

The source of the problem has been identified to be a cross-talk between calibration channels. The comparison of the data taken using the PS board with all four pulsers and with one pulser is shown in the Figs. 16 and 17. The nonlinearity for the channel 0 of the PS board is shown in Fig. 16. For the data with one active pulser, we took only one delay run. That's why we

have data every 25 ns not every nanosecond. The maximum of the nonlinearity in the channel versus channel number for the PS board is shown in Fig. 17. As can be seen even when only one FEB was active nonlinearity exceeds the 1% limit. When PS data were taken with only one pulser enabled, there is no increase in rms and the integral nonlinearity is similar to the high and medium gain levels. Low gain requires the largest available calibration signals and hence the largest current on the calibration board. This is why the cross-talk is substantially higher for these data.

6.4 Energy resolution.

There was no physics signal during FECT and therefore it was impossible to make a measurement of the most important characteristic of the system, i.e. of its energy resolution. We could make, however, a reconstruction of the DACin that plays the same role for the calibration signal as the deposited energy for the physics signal. From the parameters of the system we can calculate the current corresponding to the calibration signal and the energy that must be deposited in the cell to produce this current signal. [3] Thus, we can reconstruct DACin in units of energy (electron-volts). All following results are obtained for this reconstructed "energy".

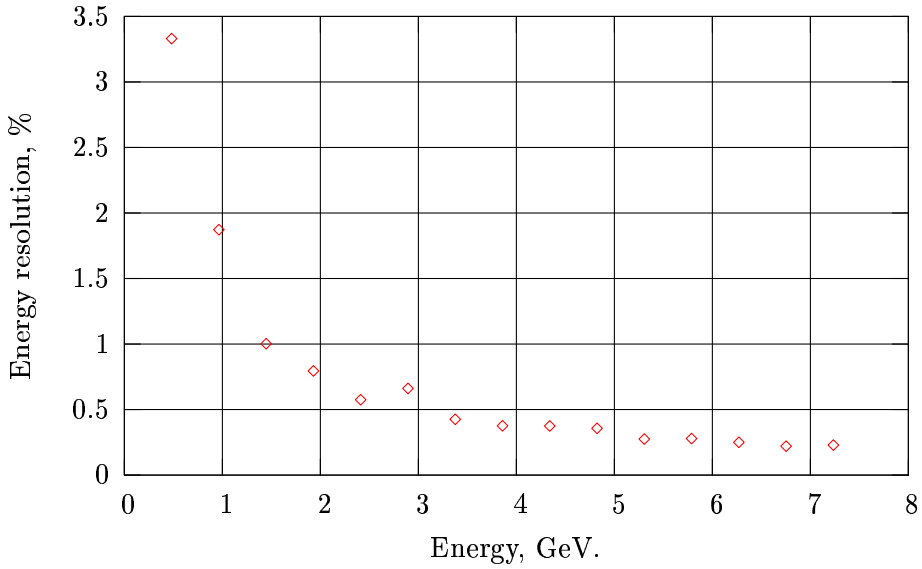

Figure 18: Example of energy resolution for high gain.

The examples of the energy resolution for the calibration signal for all three gain values are shown in Figs. 18 - 20.

Energy resolution is usually parametrized as

$$\sigma/E = a/\sqrt{E} \otimes b/E \otimes c,$$

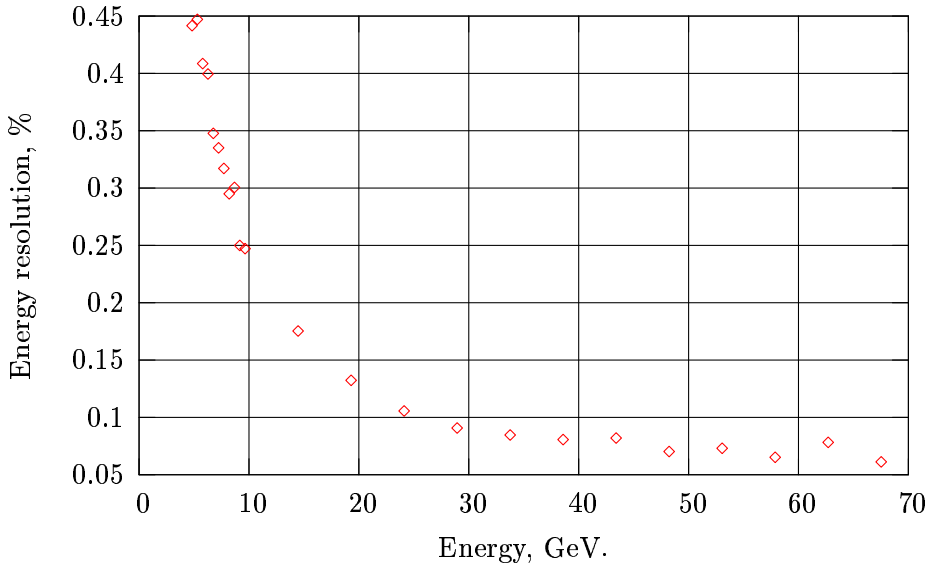

Figure 19: Example of energy resolution for medium gain.

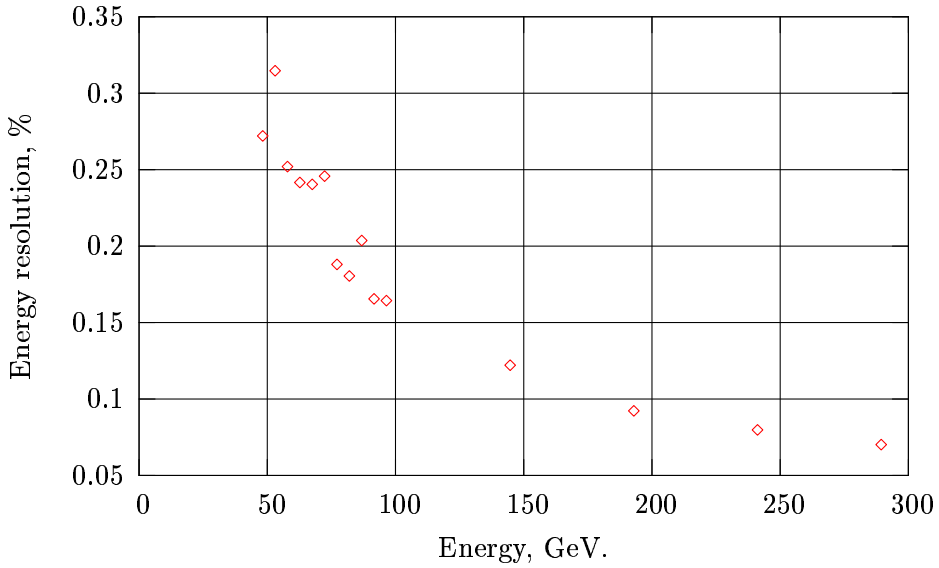

Figure 20: Example of energy resolution for low gain.

where a is a stochastic term, b is a coefficient of the noise term, and c is a constant term.

In order to reach the new physics discovery potential there are several requirements listed in the TDR [1] that describe the energy resolution, the noise and the constant terms of the calorimetric measurements. Contribution to the constant term from the electronics must be below 0.25% (total constant term must be below 0.7%). The measured values of the constant

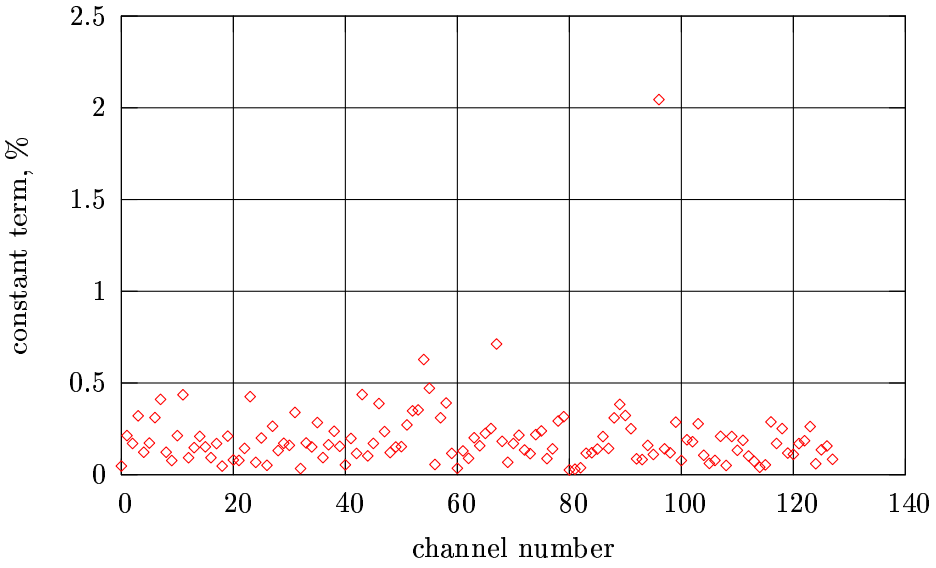

Figure 21: Constant term for high gain.

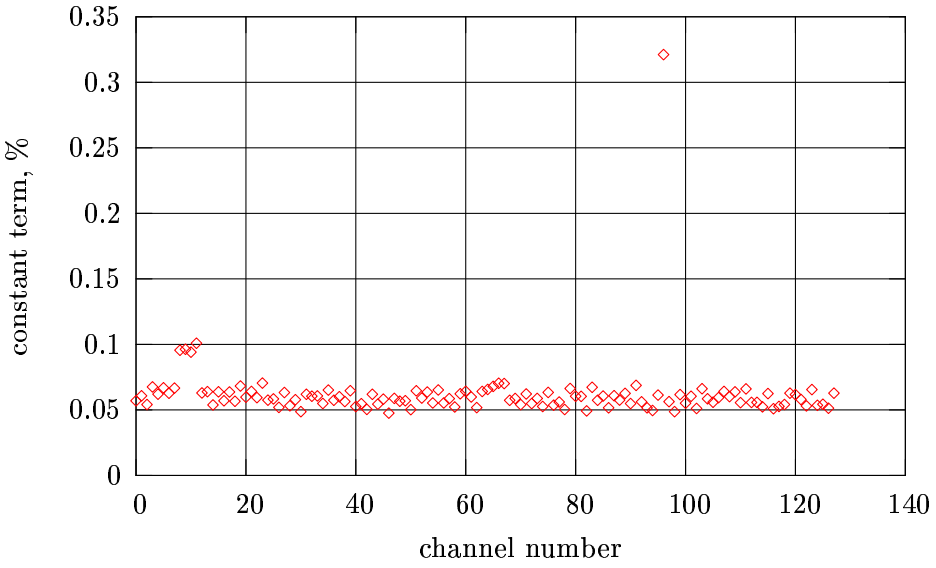

Figure 22: Constant term for medium gain.

terms for all three gains are shown in Figs. 21-23. The requirements on the noise term are less strict and the limit is below 200-400 MeV for different space positions. The noise term results are shown in Figs. 24-26. The stochastic term is defined by properties of the calorimeter itself and couldn't be investigated in the FECT because no real calorimeter cells were there.

Here I need to mention that requirements are made for energy resolution of a particle. A

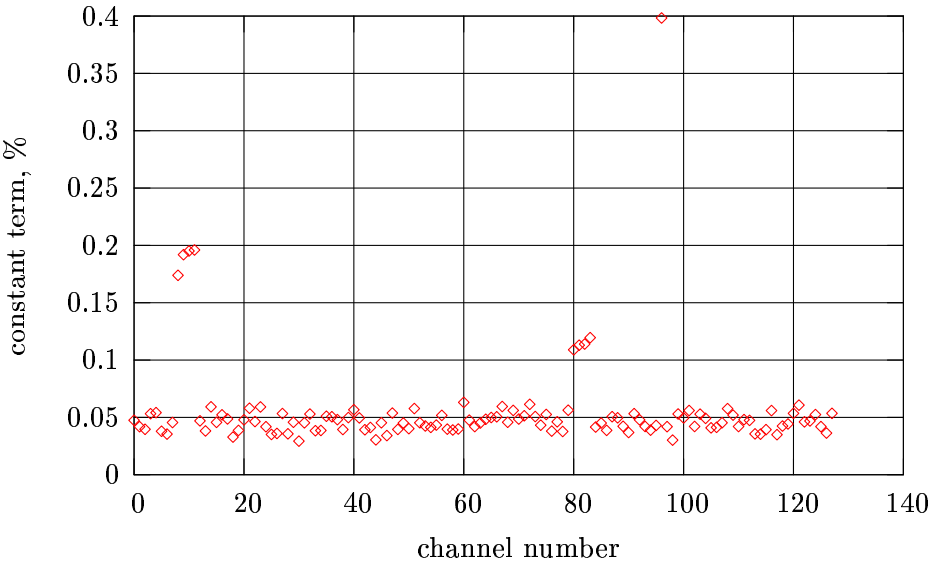

Figure 23: Constant term for low gain.

particle deposits its energy in several calorimeter cells or a cluster. All calibration results here are made for the one cell. Pileup is also not included.

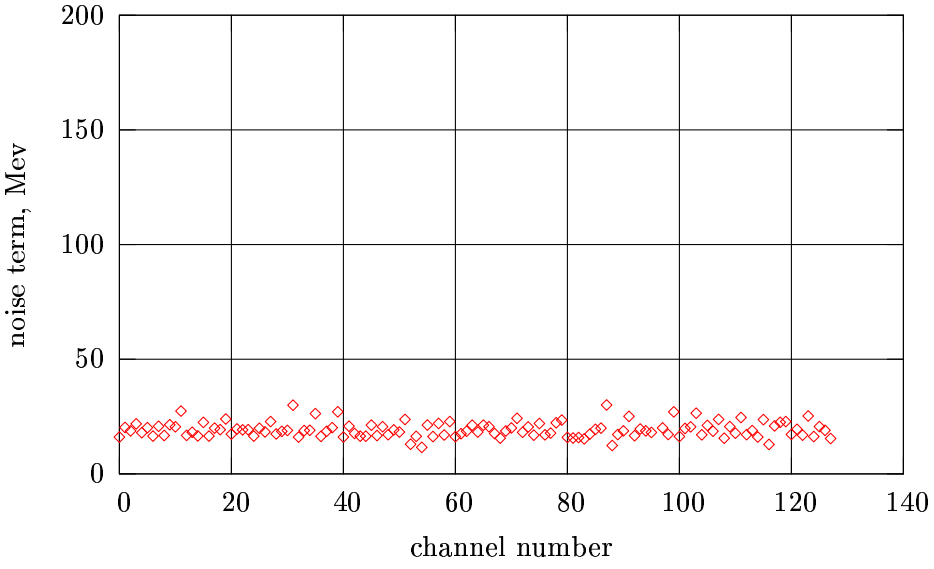

Figure 24: Noise term for high gain.

The medium gain data satisfy and exceed all requirements. The constant term for the high gain data was measured to be up to 0.5%; the TDR requirement is 0.25%. However, this result

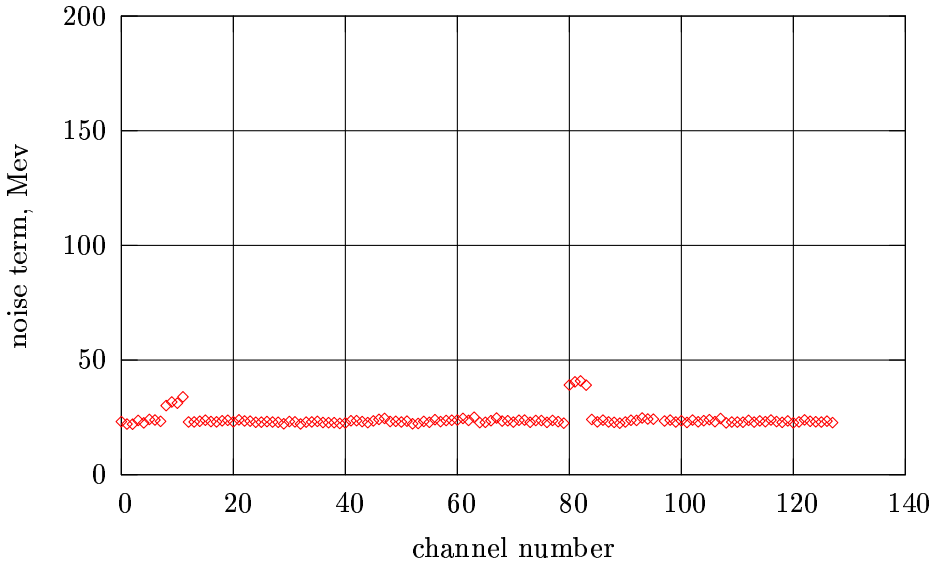

Figure 25: Noise term for medium gain.

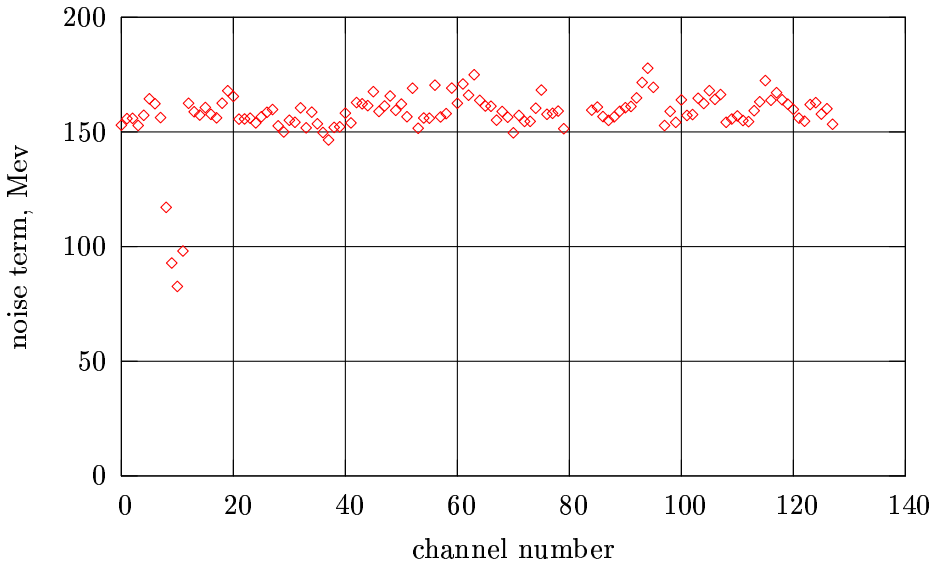

Figure 26: Noise term for low gain.

is from small signals.

The low gain data have some problems with the noise term, but they come from cross-talk between the calibration channels. The low gain data still satisfy the constant term requirements even with large cross-talk.

7 Conclusions.

The LAr calorimeter has a calibration system that was tested during the FECT. The calibration system satisfies the 1% linearity requirement for the high and medium gain data. The calibration data indicate a problem only for the PS board due to the cross-talk between calibration channels. The problem can be avoided by taking data for the PS board separately from the other boards. Similar problems exist for all boards at low gain because of large cross-talk. The reason is also a large cross-talk. It is more difficult to avoid the problem for the low gain, but taking data for one calibration channel at a time appears to satisfy the calibration condition.

The calibration procedure, which has been developed and tested during the FECT, allows the calibration of the readout electronics and meets the energy resolutions requirements of the TDR. The constant term is less than 0.25% for the medium and low gains. For the high gain it is less than 0.5%. High gain limit is less important because it corresponds to low energy deposited in the cell. When we reconstruct the energy of the particle in the cluster, contribution from the cells with high gain is small and won't affect the overall energy resolution. The noise term requirement is 200-400 MeV depending on the position of the cell. All data are inside limits, but the noise term for the low gain data is just less than 200 MeV, while the noise term for the high and medium gain data is less than 20MeV. We believe that this difference is explained by the large cross-talk for low gain data.

References

[1] ATLAS Collaboration. *ATLAS detector and physics performance. Technical Design Report.* CERN/LHCC 99-14, 1999.

[2] L. Serin D. Fournier. *Experimental techniques. LAL 96-57 July 1996.*

[3] ATLAS LARG Unit. *Liquid Argon Calorimeter Technical Design Report.* CERN/LHCC 96-41, 1996.

[4] BNL group. *FECT proposal. http* : $//larg - fect.usatlas.bnl.gov/fect_docs/fct - proposal.pdf$.

[5] E.G. Stern W.E Cleland. *Signal processing considerations for liquid ionization calorimeters in a high rate enviroment.* Nucl. Instr. and Meth. **A 338** (1994) p. 467-497.